PERGAMON

Continental Shelf Research 20 (2000) 2113–2140

CONTINENTAL SHELF RESEARCH

The role of wave-induced density-driven fluid mud flows for cross-shelf transport on the Eel River continental shelf

P. Traykovski*, W.R. Geyer, J.D. Irish, J.F. Lynch

Department of Applied Ocean Physics, Woods Hole Oceanographic Institution, Wood Hole, MA 02543, USA

Abstract

Observations of cross-shelf sediment transport conducted in the winter of 1997–1998 as part of the STRATAFORM program reveal that gravitationally forced density flows of fluid mud trapped within the thin wave bottom boundary layer provide a mechanism for forming flood deposits on the Eel river continental shelf. The data from two moored tripods located on the 20 and 60 m isobaths combined with "rapid response" hydrographic surveys, indicate a process whereby the Eel River delivers sediment on to the inner shelf faster than dispersal and transport processes are able to move it offshore. The river does not deliver sediment beyond the inner shelf because the plume is trapped along the coast due to onshore surface flow associated with downwelling favorable winds. However, the final flood deposition region is located seaward of the 50-m isobath. Acoustic backscattering data taken on the 60-m isobath (in the historic flood deposit region) show two depositional events of 6 and 13 cm during a period of high river discharge and high waves in January of 1998. These depositional events are associated with fluid mud layers that scale in thickness with the wave boundary layer. Velocity profiles from a vertical array of current meters spanning the bottom 2 m of the water column show that the current meter closest to the seafloor has the largest offshore velocity during the depositional events, indicating an offshore flow of the fluid mud from the inner shelf to the flood deposit region. During periods of low concentration suspended sediment transport without fluid mud layers present, either no deposition or erosion was found indicating that the offshore flow of the fluid mud is the dominant depositional mechanism.
© 2000 Elsevier Science Ltd. All rights reserved.

Keywords: Eel River; Sediment transport; Fluid mud; Sediment gravity flows; Sediment dynamics; Shelf sedimentation

*Corresponding author.
E-mail address: ptraykovski@whoi.edu (P. Traykovski).

0278-4343/00/$ - see front matter © 2000 Elsevier Science Ltd. All rights reserved.
PII: S0278-4343(00)00071-6

1. Introduction

The location of deposits of riverine sediments on the continental shelf depends critically on the transport and dispersal mechanisms that deliver sediment to the coastal ocean. Whereas coarse sediment settles rapidly out of a fresh-water river plume, fine sediment may travel substantial distances. On low-energy shelves, such as the Louisiana shelf off of the mouth of the Mississippi River (Wright and Coleman, 1974) or the West African shelf off the mouth of the Zaire River (Eisma and Kalf, 1984), deposition regions may be found underneath the surface plume as sediment settles directly out of the plume onto the seafloor. However, on shelves with strong currents or large waves, the final deposition region may not be located under the plume due to resuspension and transport of sediment away from the river plume in the bottom boundary layer. The continental shelf off the Eel River in Northern California is an example of a highly energetic environment with a large supply of riverine sediment during winter flood events. This dispersal system has been studied extensively in the past several years as part of the STRATAFORM (Strata Formation on Continental Margins) program (Nittrouer, 1999; Nittrouer and Kravitz, 1996).

Coring surveys of the Eel River shelf revealed that the flood deposits were located seaward of the 50 m isobath (Wheatcroft et al., 1996, 1997; Wheatcroft and Borgeld, 2000), whereas the river plume, as observed by helicopter-based hydrographic surveys, was generally located within the 40 m isobath due to downwelling favorable winds (Geyer et al., 2000) (Fig. 1). Thus it was hypothesized that sediment was transported seaward in the bottom boundary layer. In general, the bottom boundary layer transport processes that are responsible for redistributing riverine sediment range from resuspension of sediment by waves and/or strong currents and subsequent transport by the mean currents (Wiberg et al., 1994; Smith, 1977; Sternberg, 1986) to density-driven "hyperpycnal" flows of highly concentrated sediment suspensions (Wright et al., 1990; Mulder and Syvitski, 1995).

On the Eel River continental shelf, bottom boundary layer measurements of suspended sediment flux at the 50 m isobath (S-50, Fig. 1) taken during the winter of 1995–1996 revealed an offshore transport of low concentration (less than 10 g/l) suspended sediment (Cacchione et al., 1999). Other observations during the same time period taken at the 60 and 70 m isobath revealed a convergence in offshore flux between these two locations (Wright et al., 1999). This convergence of offshore suspended sediment transport is a possible explanation for the location of the flood deposit between the 60 and 90 m isobath. Two-dimensional modeling studies of the Eel River shelf have also shown a convergence in suspended sediment flux due to gradients in wave energy as a function of water depth and/or convergences in mean current velocities which could lead to offshore flood deposits of fine sediment. (Harris, 1999; Zhang et al., 1999).

However, optical backscattering sensor (OBS) measurements on the 60 m isobath during a large flood event in 1997 have shown sediment concentrations in excess of 7 g/l (Ogston et al., 1998). This is approaching the concentration level of fluid mud (typically defined as concentrations in excess of 10 g/l, Kineke et al., 1996; Ross and

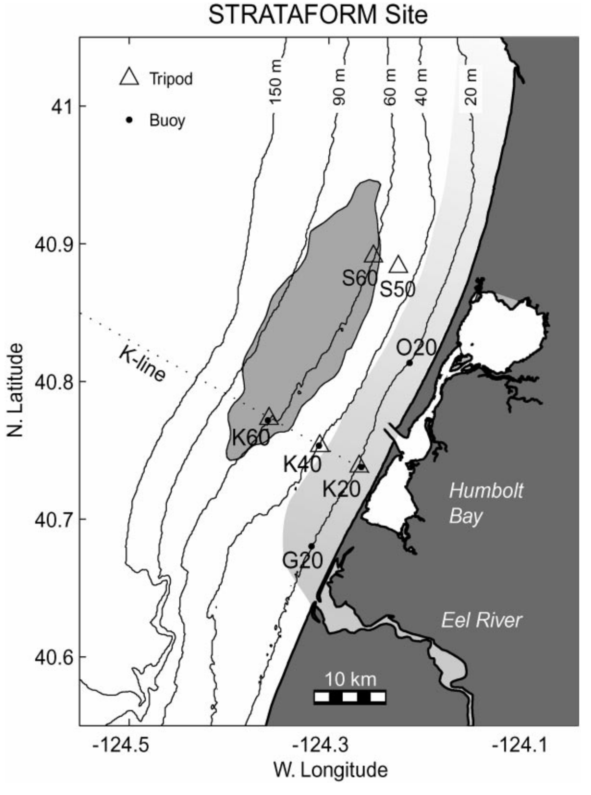

Fig. 1. (a) STRATAFORM bathymetry and the location of the three moorings and tripods deployed in the winter of 1997–1998 along the K-line. Locations of previous tripod deployments at S50 and S60 are also shown The general location of the 1995 and 1997 flood deposit is shown as the dark shaded region (Wheatcroft et al., 1996). The typical location of the Eel River plume during downwelling favorable wind (i.e. trapped against the coast within the 40 m isobath) is also shown in lighter shading. The location of the three hydrographic survey stations (G20, K20 and O20) are shown.

Mehta, 1989). Thus there is a possibility that these high sediment concentrations may provide a sufficient density anomaly to allow gravity-forced density currents (hyperpycnal currents) to exist on the Eel River continental shelf. Fluid muds have been observed at the mouths of rivers delivering large supplies of sediment, such as the Amazon (Kineke et al., 1996) and the Huanghe (Wright et al., 1990.) In both of these systems, hyperpycnal flows of the fluid mud were not directly observed, but inferred to be possible mechanisms of downslope transport based on physical modeling, as well as morphological and geochemical evidence.

To fully characterize the depositional system on the Eel River shelf it is necessary to observe the full set of processes that deliver sediment from the river mouth to its final depositional location. To accomplish this, simultaneous measurements of both the river plume and the bottom boundary layer across the shelf are required. In the winter of 1997–1998, a cross-shelf array of three moorings and three bottom

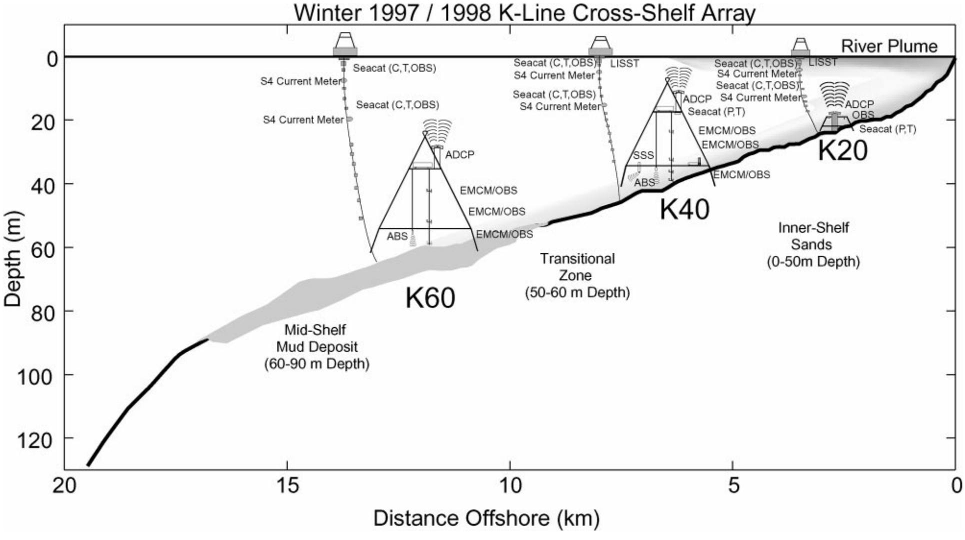

Fig. 2. Schematic sketch of the cross-shelf mooring and tripod array with bathymetry along the K-line and a conceptual diagram of the plume, bottom boundary layer suspension and flood deposit.

boundary layer instrument systems was deployed (Fig. 2). The three-dimensional structure of the plume and the inner shelf bottom boundary layer directly below the plume were resolved with "rapid response" hydrographic surveys conducted during and immediately after periods of high river discharge as described by Geyer et al. (2000) and Hill et al. (2000). These surveys also provided in situ samples of sediment concentration in the plume from water bottle samples. The goal of this paper is to identify and quantify cross-shelf transport mechanisms based on the observations from this array. The hydrographic surveys and river discharge data provide mass flux estimates to aid in quantifying the amount and spatial distribution of riverine sediment that is available to be transported across the shelf. The boundary layer measurements provide direct observations of transport processes and deposition that appear to be associated with hyperpyncal flows of fluid mud.

2. Observational techniques

2.1. Instrumentation and sampling

The cross-shelf array was deployed from November of 1997 to March of 1998 along the STRATAFORM K-line (approximately 12 km north of the Eel River mouth). Tripods and surface moorings were located at the 20, 40 and 60 m isobaths (Fig. 2). Each of the surface moorings contained an InterOceans S4 current meter at 2.0 and 6.0 m depths, and an OBS at 0.5 and 4.5 m depths, as well as a vertical array of temperature sensors. The 20 m isobath (K-20) bottom mounted tripod contained a 300 kHz RD instruments acoustic doppler current profiler (ADCP), OBS, conductivity, and temperature sensors. Unfortunately, the K-20 tripod OBS, conductivity and temperature sensors did not record any data. Likewise, the K-40 tripod, which contained a large array of sediment sensors, was destroyed (perhaps by fishing activities), partially buried, and could not be recovered.

The K-60 Tripod contained a two-frequency (2.5 and 5.0 MHz) downward aimed acoustic backscattering sensor (ABS) which recorded 1.28 m range profiles of backscattered acoustic intensity with 1 cm vertical resolution. A vertical array of Marsh-McBirney electromagnetic current meters (EMCMs) with sensors located at 0.5, 1.1 and 2.1 m above bottom (mab) was used to measure bottom boundary layer velocity profiles. A D&A Instruments OBS-3 was located adjacent to each EMCM sensor. The instruments were set to sample the surface wave frequency and lower-frequency processes by collecting data in a burst sampling mode of 8 min of 2 Hz sampling once per hour. The tripod also contained an upward looking ADCP that malfunctioned and from which data could not be downloaded. OBS sensors from the moorings and hydrographic survey were set at different gain settings from the tripod sensors and were calibrated relative to bottle samples from the surface plume.

Both the acoustic intensity profiles from the ABS and the OBS data were calibrated to relate the backscattered intensity to sediment concentration. Calibrations were performed in the lab with a sample of the bottom sediments collected from K-60 at the end of the deployment which contained less than 5% sand sized particles ($>63\,\mu m$). Maximum concentration levels for the ABS calibration were limited to several hundred milligrams per liter since a limited supply of sediment was available and the ABS calibration requires a $0.75\,m^3$ tank. The OBS sensors could be calibrated with higher concentration since a smaller bucket was used. Both acoustical and optical instruments show a linear relation with sediment concentration in the calibration tests with R^2 over 0.99 (Fig. 3).

The largest sources of error in applying these calibrations to field data are due to the size dependence of the scattering and attenuation of the acoustical or optical

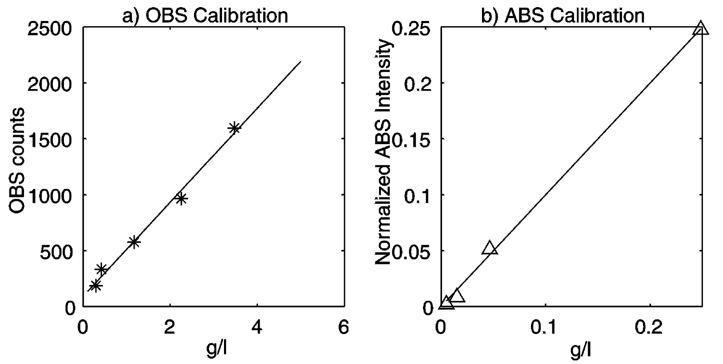

Fig. 3. (a) Tripod OBS calibration data and (b) acoustic backscattering sensor calibration data.

energy. Because optical sensors are very sensitive to particle size (with a $radius^{-1}$ dependence relating concentration to intensity) the packaging of the sediment particles into aggregates can effect the calibration procedure. Unfortunately there were no measurements of particle size in the bottom boundary layer during this deployment. Sternberg et al. (1999) measured aggregate sizes from 130 μm (their lower limit of detection; smaller particles most likely exist) to 760 μm at the S-60 site in the fall of 1995. This range would imply a possible factor of six error in applying the OBS calibrations to field data. However, in the bottom boundary layer during periods of high stress, (when most of the transport occurs) large fragile aggregates will be broken down into smaller stronger aggregates (Agrawal and Traykovski, 1999; Hill, 1998). In an attempt to simulate this in the calibration tank, the tank was vigorously stirred before taking measurements. Based on the work of Agrawal and Traykovski (1999) a reasonable estimate for the variability in mean particle size of the aggregates during transport events is approximately a factor of two, thus giving a factor of two uncertainity in the OBS calibrations.

In contrast to the optical sensors, high-frequency acoustic backscattering sensors are thought to measure the same backscattered intensity per unit concentration regardless of whether the particles are disaggregated or packaged into aggregates (Schaafsma, Pers. comm). However if there are sand fractions present in the suspension that are significantly greater than the sand fraction in the lab test this can lead to errors in applying lab calibrations to field data. The acoustic backscatter has a $radius^3$ (primary particle size, not aggregated) dependence relating concentration to intensity because the acoustic wavelength is much greater than the particle size. Drake (1999) reported that in the flood deposit layer sand size particle fractions typically composed less than 10% of the total, and that most of this sand-sized matter was non-mineral material such as plant debris (Leithold and Hope, 1999). At O-70, a temporal analysis of the evolution of the 1995 flood deposit layer showed it tended to coarsen with time after the initial emplacement, due to subsequent offshore transport of inner shelf sands (Drake, 1999; Wheatcroft et al., 1996). Since our calibration sample was taken at the end of the deployment it presumably contained more coarse material than the suspensions may have contained during the transport events associated with the river floods. A calibration sample that is coarser than the actual suspension would lead to a calibration factor that is too low and thus the sediment concentration measured by the ABS during the flood events would most likely be an underestimate of the actual concentration.

Perhaps a more significant source of error in relating calibration tank data to field data is the attenuation of acoustic energy as it propagates through high-concentration suspensions, as will be discussed in a subsequent section. This type of error also leads to an underestimation of sediment concentration. The attenuation of optical energy in the OBS measurement reduces the size of the sampling volume, which leads to a reduced backscatter at high concentrations (Kineke and Sternberg, 1992). This occurs in excess of 10–15 g/l for these sensors, based on calibration tests with similar-sized sediment from a different site. As these concentration levels were not present at the OBS sensors during this deployment, this is not a significant issue.

3. Short-term, inner-shelf sediment storage

The high river discharge events that occur in the winter months on the Eel River shelf are generally forced by rain associated with atmospheric low-pressure systems impinging on the coast from the west. This causes the high discharge events to be well correlated with strong winds from the south (Harris, 1999). These southerly winds cause along-shelf currents to the north and downwelling favorable (onshore) surface currents which trap the Eel River plume against the coast. Rapid-response hydrographic observations and OBS measurements on the cross-shelf mooring array have shown the plume to be confined landward of the 50 m isobath during downwelling favorable winds. The settling rate of sediment out of the plume is variable and depends mainly on the speed of the plume (Geyer et al., 2000). Estimates of the sediment loss from the plume reveal that 60 to70% of the sediment has settled out of the plume onto the inner shelf bottom boundary layer by the time the plume reaches the K-line (Geyer et al., 2000).

3.1. Temporal variability

Although the Eel River did not have "historic" flood events in the winter of 1998 as it did in 1995 and 1997, several floods with discharge in excess of 3000 m^3/s took place during the period between January 12 and February 11, 1998 (Fig. 4). To examine the temporal variability of sediment concentration on the inner shelf, three CTD casts from the K-20 station taken on separate days during the January 10–22

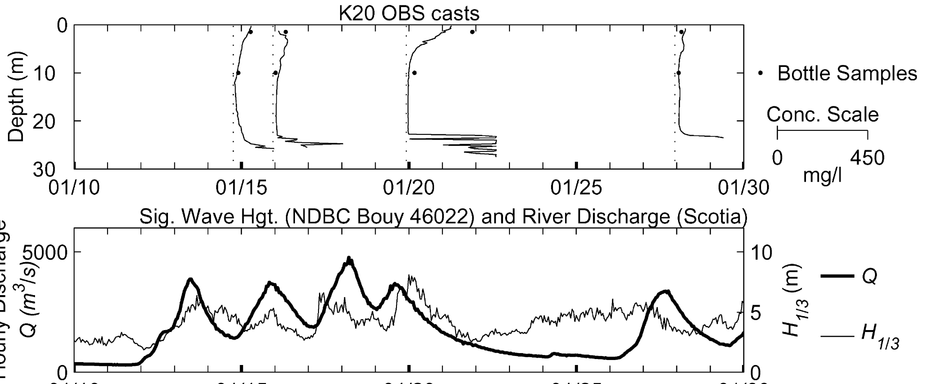

Fig. 4. (a) Rapid response OBS casts from the K-20 site. The dashed vertical axis indicates the time of the cast and the concentration is indicted by the scale on the right. The OBS sensor reached the limit of its digitization at a concentration of 450 mg/l. (b) Significant wave height, $H_{1/3}$ (Thick line, right y-axis) and river discharge, Q (thin line, left y-axis). From January 15 to 20 the bottom turbid layer thickness, increases in sediment concentration and shows an increasingly sharp gradient at the top of the layer in response to a supply of fine sediment from river discharge events that is kept in suspension by the large waves.

high-discharge event are shown in Fig. 4. The OBS profiles show concentrations of 100–300 mg/l in the surface plume with the larger values on January 20. In the bottom boundary layer on January 14, at the beginning of the event, the sediment concentration profile shows a smooth upward concave structure consistent with a gradient diffusion process of sediment being resuspended from the bottom. On January 15 the sediment concentration gradient at the top of the turbid bottom layer has sharpened considerably, and the maximum concentration has increased by a factor two to 350 mg/l. On January 20 the gradient has become very sharp, the thickness of the turbid layer has increased to 5 m, and the concentrations are above the maximum recording level of the OBS electronics of 450 mg/l. This maximum recording level is due to the fact that the OBS were set at a high gain for sensitivity to the "low" concentrations expected in the plume. However the backscatter shows several minima in the turbid layer which may be the result of very high concentrations. The OBS sensors are known to show decreased backscatter at high concentration due to high optical attenuation which reduces the sampling volume (Kineke and Sternberg, 1992) at above 10–15 g/l. Other evidence for high concentrations in the bottom boundary layer on January 20 are from the low-conductivity readings in the bottom turbid layer, as discussed in the next section.

One interpretation of the increasing concentration at the K-20 station during this high discharge event is that there is accumulation of river-derived sediment in the bottom turbid layer on the inner shelf during this period. The transport by alongshore and offshore bottom currents was not able to remove sediment from the inner shelf as fast as the river plume delivered it. To examine the other possibility, that the increase in sediment concentration was a function wave stress, the temporal variability of the significant wave height can be examined. The surface gravity waves have four broad peaks, which are roughly correlated with the peaks in discharge. From January 14–15 to January 20 the wave height increased from about 5.5–7 m. The largest peak of 8 m wave height occurred just after the sample on January 20. If the suspended sediment concentration scales approximately as wave height squared (Smith and Mclean, 1977), one could expect to see 50% more sediment on the 20th than the 14th as opposed to the order of magnitude more that is actually observed. If there had not been a series of high discharge events, the waves would have simply resuspended the predominately sandy sediments that are found on the inner shelf during periods of low discharge. Thus while wave resuspension certainly does play a role in resuspending sediment on the inner shelf, the increase in suspended sediment concentration (which leads to the formation of the highly turbid layer) observed during the period of high river discharge is most likely explained by the large supply of easily resuspended fine sediment from the Eel River plume.

3.2. Spatial variability

To examine the spatial distribution of the sediment concentration on the inner shelf, three hydrographic survey casts taken along the 20 m isobath on January 19 21 : 51–22 : 10 UTC are shown in Fig. 5. The OBS profiles reveal a 5–6 m thick turbid

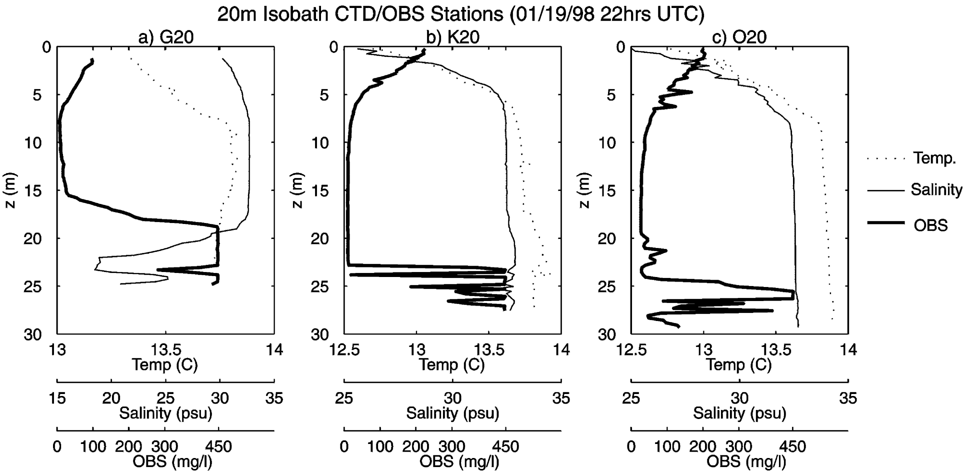

Fig. 5. The along-shelf variation of depth profiles of optical backscatter, salinity as measured by conductivity, and temperature from stations (a) G-20 (4 km from river Mouth), (b) K-20 (12 km from river Mouth) and (c) 0-20 (20 km from river Mouth). The scales for each of the three measurements are shown on the bottom of each panel and the line-type legend is on the right. The low conductivity in the bottom turbid layer present at G-20 indicates that high sediment concentrations are present in this layer.

layer with concentration in excess of the OBS maximum recording level of 450 mg/l stretching from the G-line (4 km from the river mouth) to beyond the O-line (20 km from the river mouth). Of particular interest are the profiles taken at G-20 where the conductivity sensor measures a conductivity equivalent to a salinity of 18 psu in the turbid bottom layer. While there is fresh water present in the surface plume, it is about one degree colder than the ambient seawater. Since the water mass properties are roughly conservative, if the low conductivity in the bottom layer were due to fresh water, a reduction in temperature would be expected also. The similar temperature of the turbid layer to the water immediately above it is not consistent with a riverine source. Thus the apparent low salinity is not due to river water that may have excess density due to suspended sediment.

Low conductivity can result from high suspended sediment concentration, because the sediment has conductivity that is orders of magnitude lower than seawater. To relate the decrease in conductivity to sediment concentration, Archie's law can be used:

$$\frac{\rho_{measured}}{\rho_{seawater}} = \phi^{-m}, \tag{1}$$

where ρ is the resistivity (conductivity^{-1}), ϕ is the porosity of the sediment, and m is a empirical parameter with values from 1.2 to 3 (Archie, 1942; Jackson et al., 1978). Using a conductivity equivalent to a salinity of 18 psu in Eq. (2) predicts porosities of 40–60% which are much lower than should be found in a fluid mud that the CTD package could penetrate. Porosity values of 40–60% are found 2 m below the seafloor in compacted sediment that the CTD package could not penetrate (Evans et al., 1999; Wheatcroft et al., 1996). The profiles are consistent on both the downcast and the upcast indicating that the conductivity sensor was not fouled. The pressure sensor was working correctly and indicates the instrument was not dragged on the seafloor. Clearly this use of a conductivity sensor to estimate porosity and sediment concentration needs more verification; however it does indicate that sediment concentrations are orders of magnitude higher than the OBS maximum recording limit of 450 mg/l.

A reduction in conductivity is also seen at K-20, although to a much lesser extent. The reduction in conductivity at K-20 is 2.7% indicating a porosity around 95%, which is closer to what could be expected for a high sediment concentration liquid mud layer. At the O-line no reduction in conductivity is visible. This gradient in sediment concentration with distance from the river mouth is consistent with the interpretation that the river supplies a greater amount of sediment to the inner shelf than can be dispersed into deeper water during the period from January 10 to January 20. The alternate interpretation of sediment concentration being primarily a function of wave stress would result in uniform along-shelf concentrations, because the wave stress should be approximately uniform in the along-shelf direction.

As an alternate method to estimate the concentration in this layer, the amount of sediment that is deposited into the inner shelf turbid layer from the plume (60–70% of the total discharge of $5.1–10^6$ t based on Geyer et al., 2000), in the region between the river mouth and the K-line, can be divided by the areal dimensions ($5\,km \times 12\,km$) of this region and the observed layer thickness. If the sediment mass were uniformly distributed, this calculation would result in a concentration of 12 g/l, consistent with the reduction in conductivity observed at the K-20 site. As indicated by the spatial gradient is the reduction of conductivity and OBS readings, the concentration is not uniformly distributed, but is highest closer to the river mouth. However, this estimate of sediment concentration does indicate that enough sediment is available from the river to form a short-term pool of fluid mud on the inner shelf near the river mouth.

3.3. ADCP burial on the 20 m isobath

Another observation that provides information on the amount of sediment supplied to the inner shelf is the evidence of burial of the ADCP located at K-20. The backscattered intensity from the 300 kHz ADCP shows levels around 70–80 dB with increased levels during periods of high river discharge (Fig. 6).The scattering from the sea surface is also visible in the upper range bins, and is modulated by the tides. On January 20, 1998 0300 UTC, coinciding with a peak wave height of 8 m, the ADCP backscattered intensity dropped dramatically over a period of 1 h. In the first half-hour sample after January 20, 0300, the intensity dropped to 40 dB, and by the next half-hour it had dropped to 20 dB. Over this period the pitch and roll sensors also recorded changes of 6 and 5°, respectively. After a period of about two days the intensity climbed back to levels between 30 and 40 dB. The surface return is still visible at the same mean elevation, indicating that the tripod did

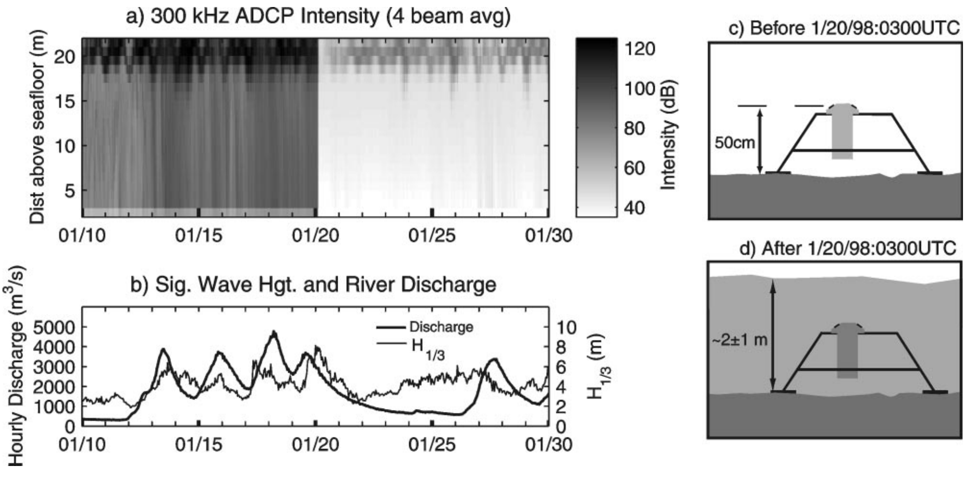

Fig. 6. (a) K-20 ADCP intensity (gray scale) vs. depth and time. (b) Significant wave height (left *y*-axis, thin line) and river discharge (right *y*-axis, thick line.) The sudden drop in intensity with no evidence for sinking of the tripod indicates the ADCP may have been buried by 1–2 m of mud on January 20 as shown in panels c and d.

not sink into the seafloor. The sediment found at K-20 during low-discharge periods is typically sandy, which, based on experience in many different sandy and energetic wave environments, only allows bottom-mounted tripods to settle a few cm.

The most likely explanation of the drop in backscattered intensity is that the tripod was buried on January 20. The amount of sediment required to bury the tripod could not have come directly from the plume. It is more likely that the tripod was buried by a large amount of sediment that had been stored on the inner shelf, landward of K-20, and was mobilized by the large waves present on January 20. It is likely that the very high concentrations that were responsible for producing the low conductivity readings on the G-20 OBS/ CTD cast on January 19, 21 : 51 played a role in the burial of the K-20 ADCP 5 h later.

The observed 50–60 dB attenuation of acoustic backscatter can be used to estimate the amount of sediment that covered the transducers. At 300 kHz, the sediment attenuation ranges from 20 to 150 dB/m depending on sediment type, with fine sands generally having the highest attenuation and clay and silt mixtures having lower attenuation (Hamilton, 1972). This produces an estimate of a sediment deposit of thickness from 30 cm to several meters plus the additional 50 cm for the transducer height. Some of the sediment below the 50 cm transducer height may have been deposited before January 20. During recovery, divers observed that the tripod was buried in ''mud'' and estimated the depth of burial to be about 1 m. This vertical scale is consistent with the acoustic data. The occurrence and timing of the burial further supports the hypothesis that the inner shelf was accumulating sediment from the river faster than it could be transported offshore.

4. Mid-shelf deposition and transport processes

The data from the tripod located on the 60-m isobath provide insight into the relationship between the river discharge, the events on the inner shelf, and the subsequent offshore transport and deposition. (Fig. 7). The downward-aimed ABS instrument provides a record of vertical profiles of sediment concentration in the bottom meter and a record of the local seabed elevation. The bottom elevation record shows a small depositional event of 6 cm on Jan 13th, a larger depositional event of 13 cm on January 20 and an erosional event of 6 cm on January 24 and January 25. The OBS sensor located 50 cm above the bottom (before the depositional events) recorded temporal peaks in suspended sediment concentration of 2–3 g/l that are correlated to combined wave and current forcing. These peaks in suspended sediment concentration at 50 cmab are also seen in the ABS data with similar concentration levels. However, what is not seen on the OBS record, but is evident in the ABS data, is a thin (10–15 cm thick), high concentration (>10 g/l) layer that appears during periods of high wave velocity (January 14–21). These concentrations are well above the commonly accepted lower limit for fluid mud of 10 g/l.

The exact concentration within this layer is difficult to estimate since the acoustic energy is significantly attenuated as it propagates into the layer. During periods of maximum concentration the attenuation is strong enough to make the acoustic return from the seafloor fall below the dynamic range of the instrument. This results in reduced backscattered intensities and reduced estimates of concentration from within the layer. The results shown in Fig. 7 do not use algorithms to correct for this, but their application is discussed in a subsequent section. However, the maximum concentration estimates of greater than 30 g/l at the top of the layer should not be strongly affected by the attenuation, and any error due to attenuation will cause the concentration to be underestimated. When the high-concentration layer is not present, the seafloor backscatters intensity equivalent to a concentration of 200–300 g/l, consistent with porosities in excess of 80–90%. Similar porosities were found in recently deposited sediment in the 1995 flood deposit layer (Wheatcroft et al., 1996). While the concentrations estimated in the fluid mud layer are greater than any of the concentrations used in the laboratory calibrations, the backscattered intensity from the fluid mud layer is an order of magnitude *less* than the backscattered intensity from the seafloor and an order of magnitude *more* than the backscattered intensity from the temporal peaks in suspended sediment concentrations of 2–3 g/l at 50 cmab.

The high concentration layer also shows a sharp interface between the fluid mud and the water above, which has concentrations of the order of 0.1 g/l. This sharp density gradient due to sediment concentration (lutocline) is a characteristic feature of fluid mud suspensions (Ross and Mehta, 1989). The lutocline weakens during periods of high mean current velocity, allowing sediment to be suspended above 50 cmab, and then it is re-established during weak currents. This is particularly evident in Fig. 7 around January 15. The turbulence associated with strong mean currents is able to overcome the density stratification at the lutocline, however the

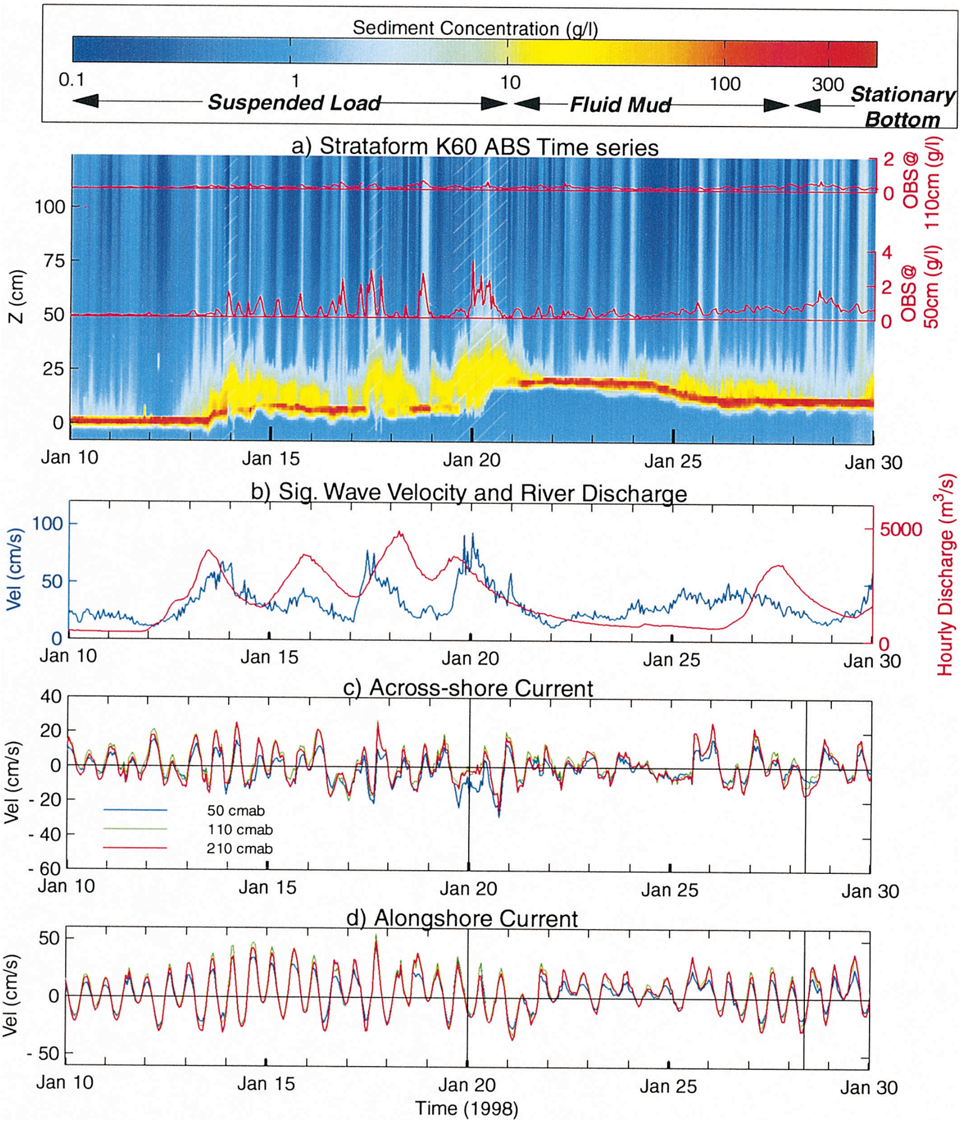

Fig. 7. (a) Time series of acoustic backscattering depth profiles. The concentration is indicated by the color scale. During the period from January 14 to 20 there exists a thin (10–20 cm thickness) layer of high-concentration fluid mud (yellow layer, with yellow corresponding to 30–50 g/l). The bottom return from the acoustics (bright red starting at 0 cm on January 10) shows two depositional events on January 14 and January 20 associated with fluid mud layers and one erosional event on January 24–26. Peaks in suspended sediment above the fluid layer are visible in both the OBS records (red lines, right y-axes) and the ABS data. (b) The fluid mud layer visible in the ABS data occurs only during periods of high wave velocities which are also associated with high river discharge events. (c) The across-shelf flows at 50, 110 and 210 cmab as measured by an EMCM array are coherent with each other and have the lowest velocities near the seafloor except during periods when a fluid mud layer is present (hatched areas). During these periods the velocity sensor closest to the seafloor has the highest velocity, in the negative direction, indicating a downslope flow of fluid mud. (d) In the along-shelf velocities the sensor closest to the seafloor consistently has the lowest velocities. Vertical lines are shown on January 20 and 28 where the ABS and EMCM are examined in more detail in Fig. 8.

turbulence associated with wave velocities is spatially restricted to the thin (~10 cm) wave boundary layer and thus does not mix sediment above this level. This effect was also noticed in fluid mud layers visible in ABS data from the S-50 site taken in 1996. The relationship between the wave boundary layer height and the lutocline is further discussed in the subsequent section.

4.1. Cross-shelf flow dynamics and evidence for density-driven flows

The vertical structure of the velocity measurements from the EMCMs suggests that the dense suspension actually drives the cross-shelf flow during periods with a fluid mud layer present. During periods when fluid mud is absent the along-shelf velocities at 50, 110, and 210 cmab are coherent with each other with sensors closer to the seafloor usually reading slightly lower velocities, as is consistent with frictional drag on the stationary seafloor (Fig. 7c). However, during some periods with a fluid mud layer present, the lowest sensor has the highest velocity in the offshore direction. This is most noticeable on January 19–20, but is also evident to a lesser degree on January 14 and 17.

The presence of an offshore flow confined to the bottom $\frac{1}{2}$ m, with increasing off-shelf velocities toward the seafloor, is strongly suggestive of a downslope flow of the fluid mud under the influence of gravity. The gravitational forcing occurs through the excess density of the 10–20 cm thick fluid mud layer which is resting on a sloping seafloor. Since no velocity measurements are available in the fluid mud layer itself, the downslope flow is inferred from measurements of velocity 50 cm above the seafloor. The moving fluid mud imposes a frictional drag on the water above it either due to mixing and the associated Reynolds stress, or due to direct viscous stress. This frictional drag forces an offshore downslope flow in the water immediately above the fluid mud layer which is seen in the current meter data.

The across-shelf bottom boundary layer dynamics can be described as a force balance between the shear stress divergence ($\mathrm{d}\tau/\mathrm{d}z$) caused by bottom friction, Coriolis acceleration ($f v_b$) and pressure gradients. The pressure gradient has two components: one associated with the larger-scale shelf dynamics which is approximate geostrophic balance with the overlying flow (with along-shelf velocity v_∞). The other is caused by the presence of the gravitation force on the excess density of the sediment suspension ($g = g\Delta\rho/\rho$) on the inclined shelf with angle sin β.

$$\frac{1}{\rho}\frac{\mathrm{d}\tau}{\mathrm{d}z} = f\Delta v + g' \sin\beta. \tag{2}$$

In the Coriolis acceleration term f is the Coriolis frequency and $\Delta v = v_b - v_\infty$ is the difference between along-shelf velocity in the boundary layer and above the boundary layer.

To determine how these dynamics control the across shelf transport of sediment two periods in the data are examined in detail (Fig. 8). The first case is data from January 20 when a fluid mud layer and increased offshore velocities near the seafloor are present (Figs. 8a and b). The second example is on January 28 when a fluid mud layer is not present (Figs. 8c and d).

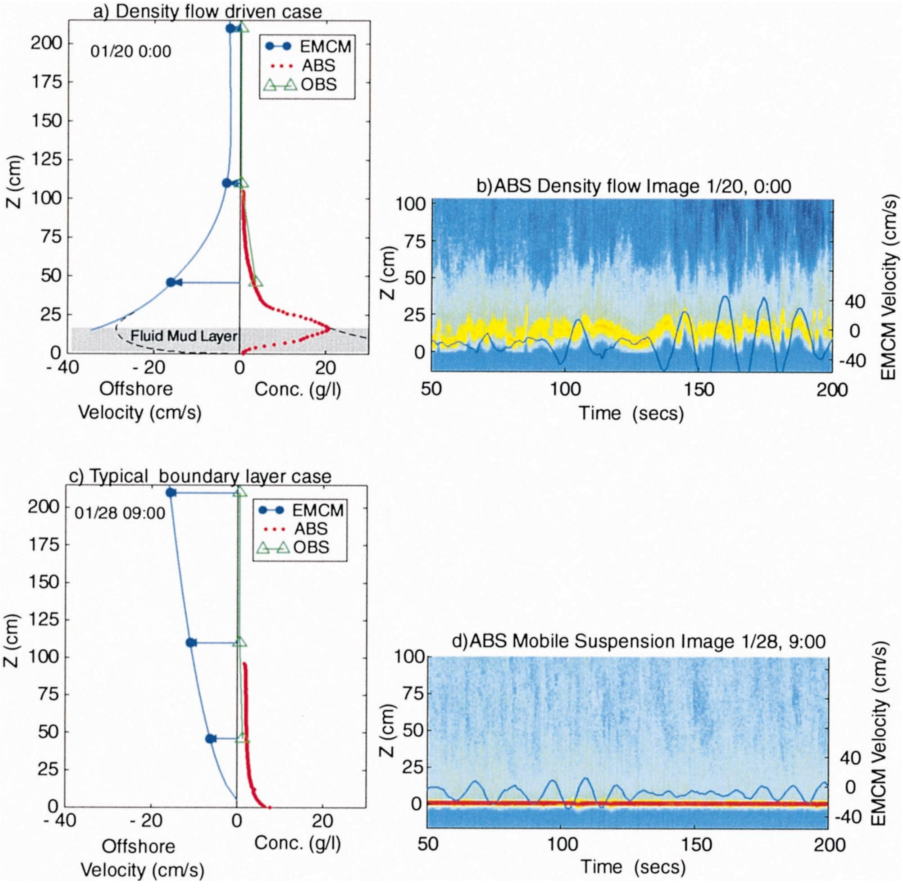

Fig. 8. (a) EMCM velocity and burst averaged OBS and ABS sediment concentration profiles taken during a downslope density flow event on January 20th and (b) a time series of acoustic backscatter depth profiles taken at the same time. The velocity profile is interpolated between data points (colored dots) and extrapolated to the top of the fluid mud layer using a piece-wise cubic spline fit. This extrapolation indicates downslope velocities of approximately 30 cm/s at the top of the fluid mud layer. The reduction of velocity through the fluid mud layer to a boundary condition of zero velocity at the seafloor (dashed line) is based on that shown by Middleton (1993) and is shown here for conceptual purposes. The reduction in the ABS concentration estimate through the fluid mud layer in due to attenuation of the acoustic energy. The acoustic data in panel a and b show a sharp density gradient at the mud–water interface with some mixing across the gradient. Instantaneous EMCM velocities from the lowest sensors is also shown as the blue line. (c) A profile taken during a typical Ekman forced offshore flow event, showing the lowest velocities near the seafloor, as consistent with frictional drag on the seafloor. In the acoustic record corresponding to this event (c and d), a diffuse suspension is seen with a weak vertical gradient.

An 8 min burst-averaged across-shelf component velocity profile taken from January 20 (Fig. 8a) clearly shows the increased offshore flow associated with the fluid mud. The velocity profile was fit with a piece-wise cubic spline and extrapolated to predict an approximately 30 cm/s offshore flow at the top of the fluid mud layer.

The piece-wise cubic spline approach was chosen since it goes through all the EMCM data points, whereas a log profile will not necessarily go through the data points. A log profile fit to the lowest two EMCM sensors results in a similar estimate of offshore velocity at the top of the fluid mud layer. The velocity profile through the fluid mud layer is based on that shown by Middleton (1993) and is shown in Fig. 8a for conceptual purposes. The maximum offshore flow, due to the gravitational forcing of the excess density of the fluid mud layer, occurs at the top of the layer. Close to the seafloor, the fluid mud velocity is assumed to go to zero due to drag on the stationary seafloor. On January 20 the ABS data (Fig. 8b) shows a sharp lutocline above a 5–15 cm thick fluid mud layer. To estimate the relative magnitudes of the forcing terms in Eq. (2) reduced gravity (g') is calculated to be $12\,\mathrm{cm/s^2}$ based on a concentration of 20 g/l, and $\sin\beta$ is estimated from *N.O.S.* bathymetry as 0.005. This results in a gravitationally forced pressure gradient of $6.0\times10^{-2}\,\mathrm{cm/s^2}$, which is a conservative estimate since the concentration in the fluid mud layer is most likely higher than 20 g/l due to the error associated with attenuation of acoustic energy. A rough upper bound for the depth-averaged fluid mud layer concentration is taken as 80 g/l since at concentration higher than this the mud becomes increasingly viscous and would not slide downslope (Ross and Mehta, 1989) The Coriolis acceleration can be estimated as $f\Delta v = 2.8\times10^{-3}\,\mathrm{cm/s^2}$ based on a Δv of 30 cm/s and an inertial frequency of f equal to 9.4×10^{-5} 1/s at this latitude. Thus the gravitational density forcing is at least twenty times the Coriolis forcing during this period. The offshore flows in the bottom $\frac{1}{2}$ m occur during periods when a fluid mud layer is present and do not correlate with periods of strong northward flow (Fig. 7d) further indicating Coriolis acceleration is not the dominant forcing mechanism for these flows.

Neglecting the relatively minor contribution of the Coriolis term, a vertical integral of Eq. (2) yields the familiar Chezy equation

$$Hg'\sin\beta = C_d U^2, \tag{3}$$

where H is the layer thickness, C_dU^2 is a parameterization of the bottom friction with C_d as the coefficient of drag including both interfacial drag from the lutocline and drag on the seafloor. Generally, the latter quantity is thought to dominate the drag (Karelse et al., 1974). For this case, H is estimated directly from the ABS data as 12 cm, and ranges from 12 to $48\,\mathrm{cm/s^2}$ based on concentrations from 20 to 80 g/l. The down slope velocity of the mud flow (U) is estimated as 30 cm/s based on EMCM data. This results in a drag coefficient of C_d = 0.0008–0.003 based on the different values for g'. If the velocity at the top of the fluid mud layer was overestimated by 5 cm/s (a maximum bound based on reasonable interpolation schemes) the C_d values would range from 0.001 to 0.005. These values are slightly less than typical values of 0.003 to 0.005 found in the literature (Johnson, 1964; Komar, 1969, 1971, 1977). Although the precise value of C_d cannot be specified, clearly there is a large enough pressure gradient due to excess density from sediment to drive the downslope flow. However, it is important to note that this gravity flow is fundamentally different from turbidity currents that have been discussed in the literature in that the high concentration described here is due to sediment trapping within the thin wave boundary layer rather than by resuspension due to the gravity current itself. As soon as the wave energy decreases, the high concentration layer ceases to exist (Fig. 7), and the sediment either settles to the seafloor if mean currents are weak, or becomes suspended throughout the bottom boundary layer if mean currents are strong. Thus an appropriate name for this type of gravity current may be a wave-induced turbidity current. Strong oscillatory motions associated with these gravity currents could either increase the drag coefficient slightly due to the interaction of current and wave generated turbulence (Grant and Madsen, 1979), or could decrease the drag due to the stratification inhibited mixing at the top of the wave boundary layer (Wiberg and Smith, 1983; Glenn and Grant, 1987).

In contrast, an across-shelf component velocity profile taken on January 28 when no fluid mud layer is present (Fig. 8c) shows decreasing velocities towards the seafloor. A time-averaged ABS profile (Fig. 8c) and ABS time series (Fig. 8d) taken at the same time shows a diffuse suspension on January 28 with a gradual vertical gradient. Maximum concentrations near the seafloor approach 6 g/l, but the averaged concentration over the bottom 2 m is 0.5 g/l. This results in a gravitation forcing of $g' \sin \beta$ equal to $1.0 \times 10^{-3}\,\mathrm{cm/s^2}$ during this period, three times less than the Coriolis acceleration estimate of $2.8 \times 10^{-3}\,\mathrm{cm/s^2}$. In this case, as in the gravity flow case, wave stresses are responsible for resuspending the sediment, but here mean currents forced by some processes unrelated to the density anomaly of the suspension (such as Coriolis acceleration or tidal pressure gradients) are responsible for the transport of sediment.

4.2. Fluid mud layer characteristics

Since fluid mud trapped within the wave boundary has not been commonly observed before and appears to be an important cross-shelf transport mechanism, the dynamics of these layers need to be better understood. While the lack of high-resolution velocity profiles through the layer limits our ability to explore the relation between the sediment stratification and the velocity shear, some insights into the dynamics of these layers can be made from the high-resolution concentration profiles measured by the ABS.

4.2.1. Mixing across the lutocline

The amount of mixing across the lutocline is important because it determines both the drag imposed on the fluid above the downslope flowing layer and the amount of sediment that is retained in the fluid mud layer. Fig. 8b indicates that there is some mixing of sediment, and presumably momentum, across the lutocline. The mixing of momentum, up to 40–60 cm above the lutocline, is the source of the increased offshore fluid velocities evident in the current meter record at 50 cmab. This mixing may be due to the mean shear produced by downslope sliding of the fluid mud. During periods when there are surface gravity wave velocities sufficient to keep the fluid mud in suspension but small mean currents, there is virtually no mixing across the lutocline (Fig. 9a), as all the sediment is trapped within the thin surface gravity wave boundary layer. Thus mixing across the lutocline is associated with strong

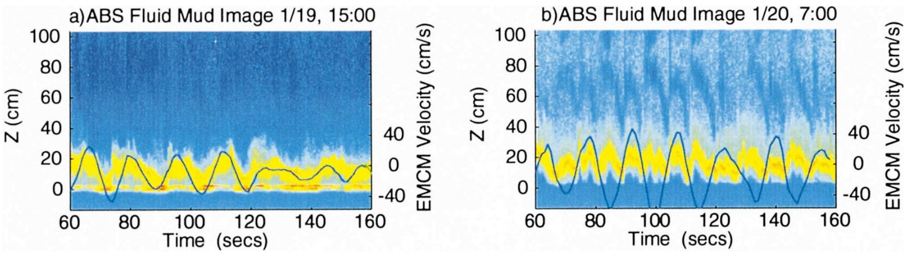

Fig. 9. (a) ABS data showing waves on the mud–water interface with very little mixing across the interface. The mud–water waves are coherent with the air–water surface gravity waves (blue, green and red lines as in Fig. 8) (b) With larger wave velocities (and orbital diameters) the mud–water waves appear at a frequency double that of the forcing.

mean flows, either due to mean currents above the fluid mud or due to mean flow of the mud itself. These mean flows lead to a boundary layer that is much thicker than the wave boundary layer, because its vertical growth is not limited by the wave frequency.

4.2.2. Wave motions on the lutocline

A prominent feature of these fluid mud suspensions is the waves that are present on the sharp density interface of the lutocline. These waves have amplitudes on the order of the layer thickness. They are not simply the result of water motion due to the surface (air–water) gravity waves, since the vertical motions associated with these surface gravity waves within 15 cm of the seafloor have amplitudes of millimeters according to linear wave theory. They appear to be forced by surface gravity waves, based on the coherence of the lutocline waves with the surface gravity waves (Fig. 9a), although sometimes there is a frequency doubling effect (Fig. 9b). This may be the result of several short wave-length lutocline waves advecting or propagating past the ABS sampling volume in each surface gravity wave period. The exact mechanism for the formation of these waves is a topic for future work. Possible mechanisms to be investigated include Kelvin–Helmholtz-type shear instabilities (Scarlatos and Mehta, 1992) or parametric resonances of the type described by Hill and Foda (1999). These waves may play a role in allowing energy through the lutocline. The generation of turbulence by the interactions of these waves with the seafloor could potentially offset the role of the stratification at the top of the wave boundary layer in limiting the amount of sediment present in the wave boundary layer.

4.2.3. Thickness of the fluid mud layer relative to the wave boundary layer

To quantify the relationship between the wave boundary layer thickness and the lutocline height, the wave boundary layer thickness can be calculated as (Wiberg and Smith, 1983; Smith, 1977)

$$\delta_w = \sqrt{f_w/8}\, a_b. \tag{4}$$

Here the wave friction factor (f_w) is calculated using the method described by Swart (1974):

$$f_w = \exp[5.213(k_n/a_b)^{0.194} - 5.977], \quad (5)$$

where a_b is the wave orbital semi-excursion amplitude near the seafloor, outside the wave boundary layer, and k_n is the hydraulic roughness. The wave orbital semi-excursion amplitude is calculated based on the significant wave properties.

To estimate the lutocline height, the vertical distance between the 10 g/l contour and the bottom location was calculated from the ABS data (Fig. 10a). Because the lutocline has waves with amplitude on the order of the layer thickness, the lutocline height was calculated based on the 2 Hz intra-burst data and then averaged over the 8 min burst length. Calculating the lutocline height based on burst-averaged concentration profiles would result in a height almost twice the intra-burst method. In order to match the temporal peaks in height of the lutocline, a hydraulic roughness of $k_n = 6$ cm was chosen. This is fairly reasonable, as hydraulic roughness can be parameterized by $k_n = 4\eta$ (Wikramanayake and Madsen, 1990) where η is ripple height. Using the formulation of 4η results in physical roughness height of 1.5 cm consistent with the results of Wright et al. (1999) based on the data from the S-60 location. It appears that the temporal variations in lutocline height are well represented by the variations in wave boundary layer thickness during periods when a fluid mud layer is present. Of course, when the wave energy is below the critical threshold for suspension, the wave boundary layer thickness does not go to zero,

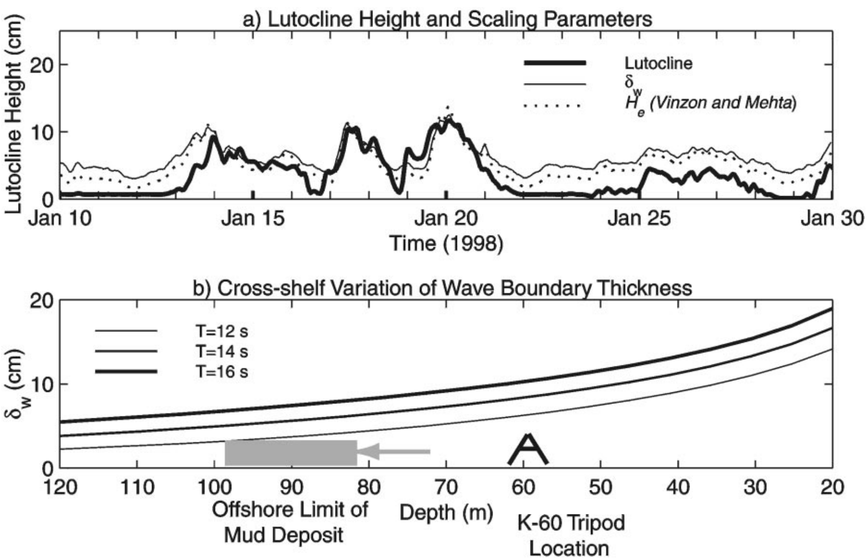

Fig. 10. (a) Temporal variation of lutocline height as defined by the 10 g/l contour, the wave boundary layer height (δ_w) and the lutocline height (H_e) as predicted by the Vinzon and Mehta model. (b) cross-shelf (depth) variation of wave boundary thickness based on linear wave theory with wave periods of 12, 14 and 16 s and wave height of 4 m.

but a wave-induced fluid mud layer is absent. During one period between January 25 and 28 when a fluid mud layer is present, the 10 g/l contour lutocline height falls slightly below the wave boundary layer and H_e scaling. This is an erosional period during which the river is not flooding (see Fig. 7), and the waves stresses are considerably smaller than during the gravity flow events of January 14–21. There is no evidence for downslope flow of fluid mud during this period. A definition of the lutocline height based on excess shear velocity above the critical shear velocity for resuspension could account for the mismatch between the lutocline height and the wave boundary layer height during low stress periods, particularly when a lutocline does not exist.

A more sophisticated approach to estimating the lutocline height under waves is described by Vinzon and Mehta (1988), who examined the balance of turbulent kinetic energy (generated at the bed by surface gravity waves) against dissipation and buoyancy flux generated by the fluid mud suspension. This analysis resulted in a lutocline height (H_e) that scales almost linearly with a_b and T (Fig. 10a), and is also temporally coherent with the observed lutocline height (as defined by the 10 g/l contour) when a fluid layer is present.

Given that the lutocline height appears to vary in a temporally coherent manner with wave energy during high stress events, the spatial changes in the lutocline height can be examined as a function of water depth based on the model that lutocline height is proportional to wave boundary layer thickness. In Fig. 10b the wave boundary layer thickness is calculated for a range of depths using the hydraulic roughness of 6 cm (which allowed the best fit to the lutocline data) combined with linear wave theory for waves of 12, 14, and 16 speriod and height of 4 m, typical of storm conditions on the Eel Shelf. As the water depth becomes deeper than 100 m, the wave boundary layer becomes thin, generally less than 5 cm thick. At the 60-m isobath station, fluid mud layers were not observed when the wave boundary layer became thinner than 5 cm. This may indicate that as the fluid mud layer slides downslope into deeper waters, at a certain depth the wave energy is insufficient to maintain the layer, and this determines the outer limit of the depositional region.

4.3. *Relative magnitude of cross-shore transport mechanisms*

In order to examine the relative magnitudes of cross-shelf transport mechanisms at the K60 site on the Eel River shelf, the sediment flux can be calculated by multiplying the concentration estimate from the ABS by a velocity profile estimated from the EMCM. During periods of relatively low concentration, the concentration profile can be estimated directly from the ABS data since acoustic attenuation is low. However, during periods with a high concentration fluid mud layer, severe attenuation of acoustic energy does not allow an accurate estimate of the concentration within the fluid mud layer. Algorithms to compensate for this, with the constraint of maintaining a temporally constant bottom return, were applied (Thorne et al., 1995). It was found that these algorithms converge poorly when the acoustic attenuation was sufficient to lower the bottom return below the minimum sensitivity of the instrument. Thus, as a conservative estimate for the concentration within the fluid mud layer, the concentration for all range bins closer to the seafloor than the bin with the maximum concentration value were set at that maximum value. This is equivalent to assuming that within the fluid mud layer there is complete mixing, which may not be physically unreasonable since there are waves on the lutocline that are the order of the layer thickness. While these waves may be irrotational, and thus cause no mixing themselves, the boundary layers associated with these large waves could be sufficient to mix the mud layer. If substantial vertical gradients within the fluid mud layer exist, the transport within this layer will be underestimated. As a rough estimate of the potential error of this technique an upper bound for the transport in the fluid mud layer was calculated by linearly interpolating the concentration profile from the bin with maximum intensity, near the top of the lutocline, to a value of 80 g/l at the seafloor.

As discussed previously, the EMCM profiles were interpolated with a piece-wise cubic spline procedure. During periods with a gravitational flow the piece-wise cubic spline fit was extrapolated to estimate the velocity at the lutocline. The velocity profile within the fluid mud layer was then estimated by a log fit that matched the estimated velocity at the lutocline and a lower boundary condition of $u=0$ at $z_0 = 0.2$ cm, consistent with the choice of $k_n = 6$ cm used in the wave boundary layer calculation. This procedure results in a mean downslope velocity profile that has its maximum value at the lutocline, consistent with laboratory and field observations of gravity currents with weak interfacial mixing. Because the errors associated with this are much less than the errors in the concentration estimates, the velocity errors are not included in the uncertainty estimate. The transport calculations were performed separately for the low concentration suspension above the lutocline, the fluid mud layer below the lutocline, and for the combined total transport. The uncertainty in the concentration estimate above the lutocline was calculated by comparing OBS and ABS data, which underestimate and overestimate concentration, respectively, based on a lab tests with potentially different sand fractions. The difference between these two estimates of concentration had a standard deviation of 20% of the mean concentration values during periods of active transport.

The results of the cross-shelf transport calculations for the months of December 1997 and January 1998 are shown in Fig. 11a in terms of a cumulative transport flux, with the negative direction oriented offshore. Due to the particular sequence of events in this time period, the cross-shelf transport of low concentration suspended sediment turns out to be relatively small (2×10^5 g/cm), as almost equal amounts of sediment are advected both onshore and offshore. The cross-shelf transport in the fluid mud layer is dominated by gravity flow events between January 14 and 20. These account for the majority (at least 80% because the fluid mud transport estimate is conservative) of the cross-shelf transport during the two-month period. Perhaps more significantly from a stratagraphic point of view, the only increases in bottom elevation (i.e. the depositional event of $+6$ cm on January 15 and of $+13$ cm on January 20) were associated with down-slope gravity flows (Fig. 11b). The erosional event (-7 cm) of January 25 and 26 was dominated by largely low-concentration suspended sediment transport in the along-shelf direction.

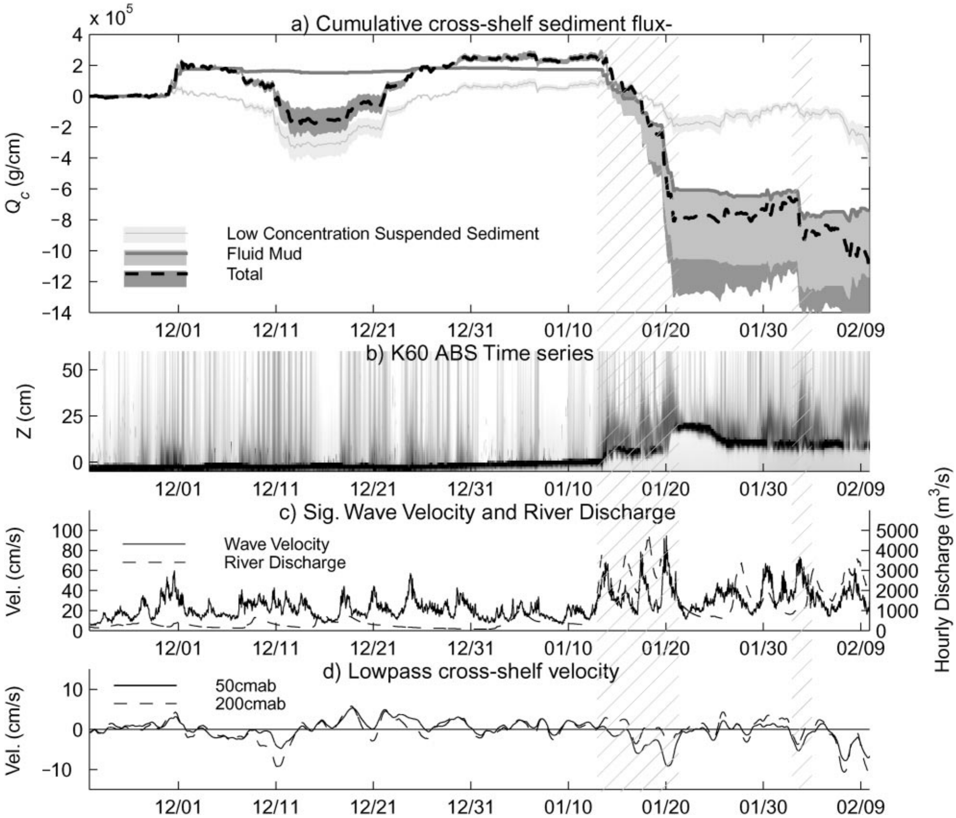

Fig. 11. (a) Cumulative cross-shelf sediment transport flux below the lutocline (in the fluid mud layer), above the lutocline (suspended transport) and the combined transport. Shaded areas represent uncertainty estimates. The transport estimate in the fluid mud layer is a conservative estimate due to attenuation and possible grain size dependence, thus the uncertainty estimate is skewed toward larger values of transport. Negative values indicate offshore transport. The cross-shelf transport is dominated by the density flow events (hatched area) on January 14–20, 1998. (b) ABS time series for the entire deployment period from the K-60 site showing positive elevation changes (deposition) only during gravity flow events d. (b) Significant wave height and Eel River Discharge. (c) Low-pass filtered (25 h) EMCM cross-shelf velocities at 50 and 200 cmab.

Fluid mud was not only associated with gravitational flows during floods. There were several periods during late November and early December in which a fluid mud layer was formed by large wave velocities (Fig. 11c). During these events there was no gravity flow signature in the velocity profiles (Fig. 11d). In fact, just before December 1, fluid mud (based on the 10 g/l definition) is transported onshore due to forcing by mean currents. These events were not associated with heavy rainfalls and the river discharge remained low. Thus it appears that large wave velocities are able to resuspend the fine sediment available at the K-60 site and create a fluid mud layer; however, in order for the fluid mud layer to slide downslope as a wave-induced gravity flow, the input of river sediment on the inner shelf is required. After January 25 there were several periods of elevated river discharge and high waves, which resulted in fluid mud layers and a velocity structure indicative of a small gravity flow just before February 4. These events after January 25 did not result in any net deposition. This may be due to the fact that although the river water discharge is relatively high, less sediment is leaving the river due to the change in the rating curve after the first major flood event of the winter season as discussed in Geyer et al. (2000). Although a thin fluid mud layer may be present at the K-60 site when there are large wave velocities, this does not necessarily imply that there will be a depositional event. However, every depositional event in the ABS time series is associated with a wave-induced gravity flow.

In the along-shore direction there was no gravity flow transport evident in the fluid mud layer, thus the total transport was due to low-concentration suspended sediment transport. Over the two-month period there was slightly more transport to the north (about 2×10^5 g/cm, similar to the cross-shelf low-concentration suspended transport). As was the case with the cross-shelf transport of low-concentration suspended sediment, the northerly transport was nearly balanced by southerly transport. The transport before December 26 was largely to the south with a magnitude of 16×10^5 g/cm, which was then balanced by largely northward transport after December 26 of 18×10^5 g/cm.

4.4. Approximate mass balances

It is instructive to put these cross-shelf transport measurements at K-60 in the context of the deposition of 19 cm of sediment between January 10 and 24 and subsequent erosion of 6 cm between January 24 and 30. Although there are no measurements of transport convergence, a convergence scale of 3–4 km in cross-shelf direction at the K-line can be inferred from seabed observations of previous flood deposits as mapped by Wheatcroft et al. (1996). Over the period of January 10–24, an estimated 8×10^5 g/cm of sediment were transported in the across-shelf direction past the K-60 tripod. Based on the position of previous years' flood deposits one would expect that $\frac{1}{2}$ to $\frac{2}{3}$ of the sediment was transported past K-60 and the remaining $\frac{1}{3}$ to $\frac{1}{2}$ was deposited shoreward. Thus dividing the total flux past the K-60 tripod (8×10^5 g/cm) by $\frac{1}{2}$ to $\frac{2}{3}$ of the patch width (3×10^5 cm) and an assumed deposit density of 0.3 g/cm^3, based on a porosity of 90%, results in a deposit of thickness 13–17 cm. The measured deposition was 19 cm thus the estimate is well within the uncertainty of the convergence scales of sediment flux. The 19 cm deposit was eroded to 13 cm by along-shelf (northward) transport after January 24, suggesting that the initial locus of the deposit was to the southern end of the previous years' deposit region, and subsequent along-shelf transport spread it to the north.

Wheatcroft et al. (1997) estimated that in the 1995 flood events the mid-shelf flood deposit accounted for 25% of the sediment discharge from the river. If this estimate of 25% is applied to the 1998 event a spatially uniform layer of approximately 3 cm thickness would have been deposited on the mid-shelf. This is based on 25% of the total river sediment discharge during January 10–24 of $4.7 \pm 2.0 \times 10^6$ metric tons (based on estimates of Geyer et al., 2000), divided by the spatial area of the deposition area from previous flood deposits ($5 \times 25\,\text{km}^2$) and the assumed density of the deposit (300 g/l). If only the sediment that was not transported past the K-line in the river plume is considered this layer thickness estimate can be scaled by 60–70% (Geyer et al., 2000) resulting in spatially uniform deposit of 2 cm. However, a net deposition of 13 cm was measured at the K-60 site in 1998. The locus of maximum deposition in the previous years' flood deposits was located several kilometers to north of K-60 and the deposit thickness at K-60 was about half of the maximum. If this spatial distribution combined with the measured deposition of 13 cm is applied to the 1998 event this would imply that a substantially larger fraction than 25% of the total river discharge is deposited in the mid-shelf flood deposit.

A possible explanation for the apparent contradiction betwen the 25% estiamte and the measured deposition of 19 cm is subsequent erosion and reworking of the sediment deposit. Although a net deposition of 13 cm was observed at the K-60 site from late November of 1997 to early February of 1998, coring work performed in the early summer did not reveal a well-defined flood deposit in 1998 as had been observed in 1995 and 1997. Rather, a bed that reflected storm reworking was found along the 60-m isobath (Drake, Pers. comm.). Thus there must have been additional erosional or reworking events after the end of the tripod deployment, but before the coring cruises that removed the flood deposit that had formed in January. A similar sequence of events may have occurred during the 1995 flood events in which Wheatcroft et al. (1997) estimated that 25% of the river sediment discharge was deposited in the mid-shelf flood deposit. The exact sequence of depositional and erosional events that occurred between the flood events and the mapping of the deposits in 1995 was not measured, however there were several periods of 3–4 m waves between the flood events in January of 1995 and the coring cruise in February. If gravity flow processes were also the dominant cross-shelf transport mechanism during that event the flood deposit may have contained a larger fraction of the riverine sediment for a short period of time until subsequent storms resuspended and dispersed it.

5. Interpretations and conclusions

On the Eel River continental shelf, recently collected data from a cross-shelf instrument array suggest that downslope, wave-induced, sediment-laden gravity currents may play an important role in the formation of the mid-shelf mud deposit. The data from the cross-shelf array combined with inner-shelf rapid response hydrographic survey work document a sequence of events suggesting cross-shelf flows of fluid mud. First, the river discharges sediment onto the inner shelf at a rate faster than it can be transported across the shelf into deeper water. This riverine sediment is stored temporarily on the inner shelf, either in the bottom boundary layer or as a temporary inner shelf deposit. This period of temporary storage lasted about one week. During this period of inner shelf storage, the hydrographic data showed a bottom turbid layer that increased both in thickness and sediment concentration. While the exact sequence of events on the inner shelf that led to the gravity currents observed on January 20 will remain unknown due to lack of inner shelf observations, the timing of events in deeper water relative to the events on the inner shelf suggests a gravity current flow. The fluid mud layer appears to be trapped in the surface gravity wave boundary layer, as the temporal variation in its thickness varied coherently with the temporal variation of the thickness of the wave boundary layer. In particular, the fluid mud layer only exists when wave energy is sufficient to develop a wave boundary layer thicker than about 5 cm. As the mud flows into deeper water, this suggests a process whereby the mud can flow downslope until it runs out of wave energy in a depth of 90–110 m of water. The lower limit of 90 m depth is consistent with the observed offshore extent of the mid-shelf flood deposit from the previous years' events. However, the landward boundary of the mid-shelf deposit is not constrained by this process and may be controlled by the ability of waves to resuspend material of the different grain sizes that define the sand–mud transition, as suggested by modeling studies (Harris, 1999; Zhang et al., 1999).

The fluid mud flows described here are slightly different from the gravity currents typically described in the literature. Turbidity currents are the gravity currents in which turbulence serves to keep enough sediment in suspension to provide a horizontal pressure gradient to drive a down-gradient flow (Middleton, 1993). These flows are often described as 'auto-suspending' flows in that the turbulence generated by the flow itself is sufficient to maintain the sediment in suspension (Bagnold, 1962). If the flow becomes insufficient to maintain auto-suspension it will become depositional and stop moving. The fluid mud flows observed at the STRATAFORM site are turbidity currents in the sense that the sediment is kept in suspension by turbulence. However, the turbulence generated by the surface gravity wave motions provides the source of turbulent energy rather than the velocity of the density-driven flow. These flows are also different from the "hyperpycnal river plume" flows as described by Mulder and Syvitski (1995) or Morehead and Syvitski (1999). In the hyperpycnal river plume flows, the plume has enough excess density due to high sediment concentration to become negatively buoyant as it leaves the river. This allows the hyperpycnal river plume to flow directly onto the seafloor and then downslope. In the turbidity current events observed on the Eel River margin, the plume leaves the river as a positively buoyant surface plume with relatively low sediment concentration. The sediment then settles out of the plume into the bottom boundary layer, where horizontal and vertical trapping mechanisms can result in high enough concentrations to initiate a downslope flow. This downslope flow continues to stay in suspension as a fluid mud layer due to the turbulence from surface gravity wave motions.

During the 1997–1998 deployments, transport by gravity-driven fluid mud flows strongly dominated the net across-shore transport; the transport of low-concentration suspended sediment played a minor role since the suspended transport happened to have almost equal onshore and offshore components. Moreover, in terms of predicting strata formation, it would appear that the fluid mud flow events are far more important than suspended transport, since all of the observed depositional events were associated with the fluid mud flow events. During periods of low-concentration suspended sediment transport (i.e. no fluid mud layer present) there was either erosion or no change in bottom elevation at the 60-m isobath. However, the preservation of flood deposits in the stratagraphic record depends critically on the exact sequence of depositional and erosional events.

Future studies should focus on determining the relation between short-term depositional and erosional events to the formation of strata that are preserved in the geological record. Studies such as this one have revealed that depositional events take place on the time scales of hours to days. This requires measuring both depositional and erosional rates on a rapid time scale with sufficient spatial coverage, and observing the dynamic processes that control these depositional and erosional events. In particular, the role of wave-induced fluid mud layers as across-shelf transport mechanism should be examined in other locations with a large supply of fine sediment, a relatively steep shelf slope and strong wave forcing.

Acknowledgements

The authors would like to thank Dr. Joe Kravitz and the Office of Naval Research (ONR) for support of the STRATAFORM program. This work was funded under ONR Code 1125GG grant N00014-94-10331. We also thank other STRATAFORM investigators, who have contributed to many useful discussions. This is Woods Hole Oceanographic Institution Contribution Number 10182.

References

Agrawal, Y.C., Traykovski, P., 1999. Particles in the bottom boundary layer: concentration and size dynamics through events. Journal of Geophysical Research, submitted for publication.

Archie, G.E., 1942. electrical resistivity log as an aid in determining some reservoir characteristics. Journal Petroleum Technology 5, 1–8.

Bagnold, R.A., 1962. Auto-suspension of transported sediment: turbidity currents. Proceedings of the Royal Society of London 265A, pp. 315–319.

Cacchione, D.A., Wiberg, P.L., Lynch, J., Irish, J., Traykovski, P., 1999. Estimates of suspended-sediment flux and bedform activity on the inner portion of the Eel continental shelf. Marine Geology 154, 83–97.

Drake, D.E., 1999. Temporal and spatial variability of the sediment grain-size distribution on the Eel shelf: the flood layer of 1995. Marine Geology 154, 169–182.

Eisma, D., Kalf, J., 1984. Dispersal of Zaire River suspended matter in the estuary and the Angola Basin. Netherlands. Journal of Sea Research 17, 385–411.

Evans, R.L., Law, L.K., Louis, B.St., Cheesman, S., Sanaikone, K., 1999. The shallow porosity structure of the Eel Shelf, northern California: results of a towed electromagnetic survey. Marine Geology 154, 211–226.

Geyer, W.R., Hill, P., Milligan, T., Traykovski, P., 2000. The structure of the Eel River plume during floods. Continental Shelf Research 20, 2067–2093.

Glenn, S.M., Grant, W.D., 1987. A suspended sediment stratification correction for combined wave and current flows. Journal Geophysical Research 92 (8), 8244–8264.

Grant, W.D., Madsen, O.S., 1979. Combined wave and current interaction with a rough bottom. Journal Geophysical Research 84, 797–1808.

Hamilton, E.L., 1972. Compressional-wave attenuation in marine sediments. Geophysics 37 (4), 620–646.

Harris, C.K., 1999. The importance of advection and flux divergence in the transport and redistribution of continental shelf sediment. Ph.D. Dissertation, University of Virginia. January, 1999.

Hill, D.F., Foda, M.A., 1999. Effects of viscosity and elasticity on the nonlinear resonance of internal waves. Journal of Geophysical Research 104 (C5), 10 951–10 958.

Hill, P.S., Milligan, T.G., Geyer, W.R., 2000. Controls on effective setting velocity in the Eel River flood plume. Continental Shelf Research 20, 2095–2111.

Hill, P.S., 1998. Destruction of macroaggregates by energetic wave forcing in a continental shelf bottom boundary layer. Eos Transactions, American Geophysical Union 79 (1).

Jackson, P.D., Taylor-Smith, D., Stanford, P.N., 1978. Resistivity-porosity-particle shape relationships for marine sands. Geophysics 43, 1250–1268.

Johnson, M.A., 1964. Turbidity currents. Oceanography and Marine Biology Annual Review 2, 31–43.

Karelse, M., Vreugdenhil, C.B., Delvigne, G.A.L., 1974. Momentum and mass transfer in stratified flows: reports on literature study. Report 880, Delft Hydraulics Laboratory, Delft, the Netherlands, 143 pp.

Kineke, G.C., Sternberg, R.W., Trowbridge, J.H., Geyer, W.R., 1996. Fluid-mud processes on the Amazon continental shelf. Continental Shelf Research 16 (5/6), 667–696.

Kineke, G.C., Sternberg, R.W., 1992. Measurements of high concentrations suspended sediments using the optical backscatterance sensor. Marine Geology 90, 159–174.

Komar, P.D., 1969. The channelized flow of turbidity currents with application to Monterey Deep-Sea Fan Channel. Journal of Geophysical Research 74 (18), 4544–4558.

Komar, P.D., 1971. Hydraulic jumps in turbidity currents. Geological SocietyAmerican Bulletin 82, 1477–1488.

Komar, P.D., 1977. Computer simulation of turbidity current flow and the study of deep-sea channels and fan sedimentation. In: Goldberg, E.D., McCave, I.N, O'Brien, J.J., Steele, J.H. (Eds.), The Sea, Vol. 6, Marine Modeling. Wiley, New York, pp. 603–621.

Leithold, E.L., Hope, R.S., 1999. Deposition and modification of a flood layer on the northern California shelf: lessons from and about the fate of terrestrial particulate organic carbon. Marine Geology 154, 183–196.

Middleton, G.V., 1993. Sediment deposition from turbidity currents. Annual Review Earth and Planetry Science 21, 89–144.

Morehead, M.D., Syvitski, J.P., 1999. River-plume sedimentation modeling for sequence stratigraphy: application to the Eel margin, northern California. Marine Geology 154, 29–41.

Mulder, T., Syvitski, J.P.M., 1995. Turbidity currents generated at river mouths during exceptional discharges to the world oceans. Journal of Geology 100, 525–544.

Nittrouer, C.A., 1999. STRATAFORM: overview of its design and synthesis of its results. Marine Geology 154, 3–12.

Nittrouer, C.A., Kravitz, J.H., 1996. STRATAFORM: A program to study the creation and interpretation of sedimentary strata on continental margins. Oceanography 9, 146–152.

Ogston, A.S., Sternberg, R.W., Cacchione, D.A., Guerra, J.V., 1998. Along-shelf Progression of River Flood Suspended Sediments on the Northern California Shelf. Ocean Sciences Meeting San Diego, February, 1998.

Ross, M.A., Mehta, A., 1989. On the Mechanics of lutoclines and fluid mud. Journal of Coastal Research, special issue 5, 51–61.

Scarlatos, P.D., Mehta, A.J., 1992. Instability and entrainment mechanisms at the stratified fluid mud-water interface, nearshore and estuarine cohesive sediment transport. Pacific Rim Congress 42, 205–223.

Smith, J.D., 1977. Modeling of sediment transport on continental shelves. In: Goldberg, E.D., McCave, I.N., O'Brien, J.J., Steele, J.H. (Eds.), The Sea, Vol. 6, Marine Modeling, Wiley, New York, pp. 539–577.

Smith, J.D., Mclean, J.R., 1977. Spatially averaged flow over a wavy surface. Journal of Geophysical Research 82, 1735–1746.
Sternberg, R.W., Berhane, I., Ogston, A.S., 1999. Measurement of size and settling velocity of suspended aggregates on the northern California continental shelf. Marine Geology. 154, 43–53.
Sternberg, R.W., 1986. Transport and accumulation of river derived sediment on the washington continental shelf, USA. Journal of the Geological Society of London 143, 945–956.
Swart, D.H., 1974. Offshore sediment transport and equilibrium beach profiles. Publ. 131, Delft Hydr. Lab., Delft, Netherlands, 1974.
Thorne, P.D., Holdaway, G.P., Hardcastle, P.J., 1995. Constraining acoustic backscatter estimates of suspended sediment concentration profiles using the bed echo. Journal of the Acoustical Society of America 98 (4), 2280–2288.
Wiberg, P.L., Smith, J.D., 1983. A comparison of field data and theoretical models for wave-current interactions at the bed on the continental shelf. Continental Shelf Research 2 (2/3), 147–162.
Wiberg, P.L., Drake, D.E., Cacchione, D.A., 1994. Sediment resuspension and bed armouring during high bottom stress events of the northern California inner continental shelf: measurements and predictions. Continental Shelf Research 10 (14), 1191–1219.
Wikramanayake, P.N., Madsen, O.S., 1990. Calculation of Movable Bed Friction Factors C.E.R.C. Tech. Prog. Rep. No. 2, Dredging Research Program, U.S. Army Corps of Eng.
Wheatcroft, R.W., Borgeld, J.C., 2000. Oceanic flood deposits on the northern California shelf: large-scale distribution and small scale physical properties. Continental Shelf Research 20, 2163–2190.
Wheatcroft, R.W., Sommerfield, C.K., Drake, D.E., Borgeld, J.C., Nittrouer, C.A., 1997. Rapid and Widespread dispersal of flood sediment on the northern California margin. Geology 254 (2), 163–166.
Wheatcroft, R.W., Borgeld, J.C., Born, R.S., Leithold, E.L., Nittrouer, C.A., Sommerfield, C.K., 1996. The anatomy of an oceanic flood deposit. Oceanography 9 (3), 158–162.
Wright, L.D., Kim, S.C., Friedrichs, C.T., 1999. Across-shelf variations in bed roughness bed stress and sediment suspension on the northern California shelf. Marine Geology 154, 99–116.
Wright, L.D., Wiseman Jr., W.J., Yang, Z.S., Bornhold, B.D., Keller, G.H., Prior, D.B., Suhayda, J.N., 1990. Processes of marine dispersal and deposition of suspended silts off the modern mouth of the Huanghe (Yellow River) 10 (1), 1–40.
Wright, L.D., Coleman, J.M., 1974. Mississippi river mouth processes: effluent dynamics and morphological development. Journal of Geology 82, 751.
Vinzon, S.B., Mehta, A.J., 1988. Mechanism for formation of lutocline by waves. Journal of Waterway, Port, Coastal, and Ocean Engineering 124 (3), 147–149.
Zhang, Y., Swift, D.J.P., Fan, S., Niedoroda, A.W., Reed, C.W., 1999. Two-dimensional numerical modeling of storm deposition on the continental shelf. Marine Geology 154, 155–167.